

# Numerical Simulation of Three Dimensional Free Surface Flows with Bubbles

Alexandre Caboussat<sup>1</sup>, Vincent Maronnier<sup>2</sup>, Marco Picasso<sup>1</sup>, and Jacques Rappaz<sup>1</sup>

<sup>1</sup> Institut de Mathématiques, Ecole Polytechnique Fédérale de Lausanne, 1015 Lausanne, Switzerland.

<sup>2</sup> Calcom SA, Parc Scientifique, 1015 Lausanne, Switzerland.

**Abstract.** A numerical model is presented for the simulation of free surface flows. The unknowns are the volume fraction of liquid, the velocity and pressure in the liquid and the pressure in the bubbles of gas which can appear in the liquid flow.

The volume fraction of liquid satisfies an advection equation, the pressure in each bubble is uniformly constant in space but depends on time and is computed using the ideal gas law, the velocity and pressure in the liquid satisfy the incompressible Navier-Stokes equations, the gas pressure being imposed as a normal force on the liquid-gas interface.

The numerical method is similar to the one described in [12,13], advection and diffusion phenomena being solved on two different grids. Numerical results in the frame of mould filling show that the effect of pressure in the bubbles of gas surrounded by the liquid cannot be neglected.

## 1 Introduction

Industrial processes such as casting, injection or extrusion involve complex free surface phenomena that can nowadays be solved numerically using commercial codes. In three dimensional situations, the motion of the free surface is generally too complex to be handled by front-tracking [10] or Lagrangian methods [7,8,18]. The Arbitrary Lagrangian-Eulerian method is also difficult to implement since the selection of the mesh velocity is nontrivial for complex flows.

An alternative is to consider the Eulerian approach, which consists in using a fixed mesh but adding an unknown function  $\varphi$  which is, in our case, the characteristic function of the liquid domain. In the level set approach [1,26] or in the pseudo-concentration method [3,4,11,17,28,29], the function  $\varphi$  is smooth. The velocity and pressure in the liquid and the gas generally satisfy the incompressible Navier-Stokes equations. Therefore the compressibility effect of gas is neglected.

In this paper, the function  $\varphi$  is the volume fraction of liquid (in fact the liquid characteristic function). It has value one in the liquid region, zero in the surrounding gas and jumps across the interface. The most famous numerical implementation of this model is the so-called Volume Of Fluid (VOF)

method, which was originally devised for finite volumes [9] and recently extended to finite elements [16]. The major difficulty in solving this problem is then due to the fact that the volume fraction of liquid  $\varphi$  is discontinuous across the interface. Since the interface moves with the fluid,  $\varphi$  must satisfy (in some weak sense) the following advection equation

$$\frac{\partial \varphi}{\partial t} + \mathbf{v} \cdot \nabla \varphi = 0 \quad ,$$

where  $\mathbf{v}$  is the velocity field of the fluid governed by the incompressible Navier-Stokes equations. In our model, the velocity field  $\mathbf{v}$  is computed only in the liquid region of the cavity. The influence of the gas surrounding the liquid is taken into account by computing its pressure, which can then be applied as an external normal force onto the liquid. The pressure in the gas is computed using law of ideal gases and is constant in space in each connected component of gas. Surface tension effects are neglected as they are not important in mould filling applications.

The numerical method is the one presented in [12,13]. An implicit splitting algorithm is used to decouple advection and diffusion phenomena in Navier-Stokes equations. Then, these two phenomena are solved using two different grids. Advection phenomena (including the motion of the volume fraction of liquid and the prediction of the fluid velocity) are solved using a fixed, structured grid of cubic cells and a forward characteristic method. On the other hand, diffusion phenomena (the computation of the gas pressure and a generalized Stokes problem in the liquid) are solved using continuous, piecewise linear finite element techniques on a fixed, unstructured mesh of tetrahedrons.

Numerical results in two and three space dimensions have already been presented in [12,13]. The pressure in the bubbles of gas that may appear in the flow was neglected. The goal of this paper is to present some results when taking into account the influence of the gas pressure on the fluid.

The structure of the paper is the following. In the next section, the governing equations are presented. In Sects. three and four, time and spatial discretizations are proposed. In Sect. five, numerical simulations are presented.

## 2 The Mathematical Model

### 2.1 Governing Equations in the Liquid

The model presented in this section is described in [12,13] except the influence of the surrounding gas on the liquid. Let  $A$  be a cavity of  $\mathbb{R}^3$  in which the fluid must be confined, and let  $T > 0$  be the final time of the simulation. For any given time  $t$ , let  $\Omega(t)$  denote the region occupied by the liquid. Finally, let  $Q_T$  be the space-time domain containing the liquid and let  $\Sigma_T$  be the space-time free surface between the liquid and the surrounding gas. The notations

are reported in Fig. 1 in the frame of a two dimensional situation, namely the broken dam problem in a confined domain.

The velocity field  $\mathbf{v} : Q_T \rightarrow \mathbb{R}^3$  and the pressure field  $p : Q_T \rightarrow \mathbb{R}$  in the liquid are assumed to satisfy the time-dependent, incompressible Navier-Stokes equations in conservative form and in the presence of a gravity field  $\mathbf{g}$ , that is

$$\rho \frac{\partial \mathbf{v}}{\partial t} + \rho(\mathbf{v} \cdot \nabla) \mathbf{v} - 2\mu \operatorname{div} \mathbf{D}(\mathbf{v}) + \nabla p = \rho \mathbf{g} \quad \text{in } Q_T, \quad (1)$$

$$\operatorname{div} \mathbf{v} = 0 \quad \text{in } Q_T, \quad (2)$$

where  $\mathbf{D}(\mathbf{v}) = \frac{1}{2}(\nabla \mathbf{v} + \nabla \mathbf{v}^T)$  is the rate of deformation tensor.

Let  $\varphi : \Lambda \times [0, T] \rightarrow \mathbb{R}$  be the volume fraction of liquid. The function  $\varphi$  equals one if liquid is present and zero if it is not and so  $\varphi$  is the characteristic function of  $Q^T$ . Since the interface moves with the liquid, the function  $\varphi$  must satisfy (in a weak sense)

$$\frac{\partial \varphi}{\partial t} + \mathbf{v} \cdot \nabla \varphi = 0 \quad \text{in } Q_T. \quad (3)$$

From a Lagrangian point of view, the function  $\varphi$  is constant along the trajectories of the fluid particles. More precisely,  $\varphi(X(t), t) = \varphi(X(0), 0)$ , where  $X(t)$  is the trajectory of a fluid particle, thus  $X'(t) = \mathbf{v}(X(t), t)$ .

## 2.2 Initial and Boundary Conditions

The initial conditions are the following. At initial time, the volume fraction of liquid  $\varphi(\cdot, 0)$  is given, which defines the liquid region,

$$\Omega(0) = \{x \in \Lambda; \varphi(x, 0) = 1\};$$

see Fig. 1 for notations. The initial velocity field  $\mathbf{v}$  is then prescribed in  $\Omega(0)$ . Let us now turn to the boundary conditions for the velocity field. It is assumed that the only forces acting on the free surface are the normal forces due to the external pressure of the surrounding gas (we neglect capillary forces or surface tension); the boundary condition is,

$$-p\mathbf{n} + 2\mu\mathbf{D}(\mathbf{v})\mathbf{n} = -(P - P_{\text{atmo}})\mathbf{n} \quad \text{on } \Sigma_T, \quad (4)$$

where  $\mathbf{n}$  is the unit normal of the liquid-gas free surface oriented toward the gas,  $P$  the pressure in the gas and  $P_{\text{atmo}}$  the atmospheric pressure. For example, consider the situation of Fig. 2, namely the filling of a two dimensional S-shaped cavity (the numerical experiment is described in Sect. 5). When filling the cavity with liquid, the gas between the valve and the liquid can escape, thus  $P = P_{\text{atmo}}$  on the upper part of the liquid-gas interface. However, a fraction of gas is trapped by the liquid and cannot escape, a resulting

force acts on the lower part of the liquid-gas interface which implies that the bubble persists during experiment.

On the boundary of the liquid region being in contact with the walls (that is to say the boundary of  $\Lambda$ , see Fig. 1), two cases can be considered. The first case corresponds to noslip or inflow conditions, the three components of the velocity being imposed. In the second case, slip or zero force boundary conditions apply, according to the flow. More precisely, if the fluid pushes against the wall, then slip boundary conditions are imposed; that is, zero normal velocity and zero tangent stress. That means,

$$\begin{aligned} \text{if } (-p\mathbf{n} + 2\mu\mathbf{D}(\mathbf{v})\mathbf{n}) \cdot \mathbf{n} < 0 \quad \text{then} \\ \mathbf{v} \cdot \mathbf{n} = 0 \quad \text{and} \quad (-p\mathbf{n} + 2\mu\mathbf{D}(\mathbf{v})\mathbf{n}) \cdot \mathbf{t}_i = 0, \quad i = 1, 2, \end{aligned} \quad (5)$$

where  $\mathbf{t}_i$ ,  $i = 1, 2$ , are two unit vectors orthogonal to  $\mathbf{n}$ . On the other side, if the fluid does not push against the wall, then the force is zero. That means,

$$\text{if } (-p\mathbf{n} + 2\mu\mathbf{D}(\mathbf{v})\mathbf{n}) \cdot \mathbf{n} \geq 0 \quad \text{then} \quad -p\mathbf{n} + 2\mu\mathbf{D}(\mathbf{v})\mathbf{n} = 0. \quad (6)$$

We have considered this kind of boundary condition in order to prevent the fluid sticking onto the walls.

### 2.3 The Model in the Surrounding Gas

Consider again the case of Fig. 2. Some gas is trapped by the fluid and is compressed. In our model, the velocity in the gas is disregarded (indeed, computing the velocity field in the gas would require solving the Euler compressible equations, this being too expensive). The pressure in the gas is computed using the *ideal gas law* at constant temperature :

$$PV = nRT, \quad (7)$$

where  $P$  is the pressure in the gas,  $V$  its volume,  $n$  is the molecular fraction,  $R$  is the gas constant and  $T$  is the (constant) temperature. Moreover the pressure inside each connected component of gas is constant in space. In the following we set  $P_i(t)$  and  $V_i(t)$  the pressure and volume of bubble  $i$  at time  $t$  and consider the situations illustrated in Fig. 3 and 4. In Fig. 3 the pressure of the trapped gas at time  $t + \tau$  is computed from the relation

$$P_2(t + \tau)V_2(t + \tau) = P_2(t)V_2(t).$$

The situation of Fig. 4 is more complex since two bubbles merge. The pressure at time  $t + \tau$  is computed by taking into account the conservation of number of molecules in the bubbles. If  $n_1(t + \tau)$  is the molecular fraction of the bubble 1 at time  $t + \tau$  and  $n_1(t)$ ,  $n_2(t)$  are the molecular fractions of bubbles 1 and 2 at time  $t$ , we have  $n_1(t + \tau) = n_1(t) + n_2(t)$ .

### 3 Time Discretization: an Implicit Splitting Algorithm

As described in [12,13], a splitting algorithm is used to solve problem (1)-(3), allowing advection and diffusion phenomena to be decoupled.

Let  $0 = t^0 < t^1 < t^2 < \dots < t^N = T$  be a subdivision of the time interval  $[0, T]$ , define  $\tau^n = t^n - t^{n-1}$  the  $n$ -th time step,  $n = 1, 2, \dots, N$ ,  $\tau$  the largest time step. Given an integer  $n$ , assume that approximations  $\varphi^{n-1}$ ,  $\mathbf{v}^{n-1}$ ,  $\Omega^{n-1}$ ,  $P^{n-1}$  of  $\varphi$ ,  $\mathbf{v}$ ,  $\Omega$ ,  $P$  at time  $t^{n-1}$  respectively, are available. Then  $\varphi^n$ ,  $\mathbf{v}^n$ ,  $\Omega^n$ ,  $P^n$  are computed by means of a splitting algorithm as illustrated in Fig. 5. Firstly, two advection problems are solved, leading to a prediction of the new velocity  $\mathbf{v}^{n-1/2}$  together with the new volume fraction of liquid  $\varphi^n$ , which allows the new computational domain  $\Omega^n$  to be defined. At this step, the new volumes of gas in bubbles are known and it is possible to compute the new pressure  $P^n$  of this gas. Finally, a generalized Stokes problem is solved on  $\Omega^n$  with boundary conditions (4) (5) (6) and the velocity  $\mathbf{v}^n$  and pressure  $p^n$  are obtained.

#### 3.1 Advection Step

Solve between time  $t^{n-1}$  and  $t^n$  the two advection problems

$$\frac{\partial \mathbf{w}}{\partial t} + (\mathbf{w} \cdot \nabla) \mathbf{w} = 0 \quad , \quad (8)$$

$$\frac{\partial \psi}{\partial t} + \mathbf{w} \cdot \nabla \psi = 0 \quad , \quad (9)$$

with initial conditions

$$\begin{aligned} \mathbf{w}(t^{n-1}) &= \mathbf{v}^{n-1} \quad , \\ \psi(t^{n-1}) &= \varphi^{n-1} \quad . \end{aligned}$$

If the effect of the boundary of the cavity  $\Lambda$  is not considered, these two problems can be solved exactly, using the method of Characteristics [21–23,30,32], the trajectories of the velocity field  $\mathbf{w}$  being straight lines. Indeed, the trajectories are given by  $X'(t) = \mathbf{w}(X(t), t)$ , but since  $\mathbf{w}$  is constant along the trajectories, we have  $X'(t) = \mathbf{w}(X(t^{n-1}), t^{n-1}) = \mathbf{v}^{n-1}(X(t^{n-1}))$ . Let  $\mathbf{v}^{n-1/2}$  denote the solution of the first advection problem at time  $t^n$  ( $\mathbf{v}^{n-1/2}$  is a prediction of the velocity field),  $\mathbf{v}^{n-1/2}(x) = \mathbf{w}(x, t^n)$ . Let  $\varphi^n$  denote the solution of the second advection problem at time  $t^n$ , i.e.  $\varphi^n(x) = \psi(x, t^n)$ . We thus have

$$\mathbf{v}^{n-1/2}(x + \tau^n \mathbf{v}^{n-1}(x)) = \mathbf{v}^{n-1}(x) \quad , \quad (10)$$

$$\varphi^n(x + \tau^n \mathbf{v}^{n-1}(x)) = \varphi^{n-1}(x) \quad , \quad (11)$$

for all  $x$  belonging to  $\Omega^{n-1}$ . Once  $\varphi^n$  is known in the cavity  $\Lambda$ , then the liquid region at time  $t^n$  is defined by :

$$\Omega^n = \{y \in \Lambda; \varphi^n(y) = 1\} \quad .$$

### 3.2 The Pressure in the Bubbles

An approximation  $P_i^n$  of the pressure in bubble  $i$  at time  $t^n$ ,  $P_i(t^n)$ , is computed following the description of Sect. 2.3. Each connected component of gas is obtained from a *coloration algorithm* described hereafter (see Fig. 6).

Let  $k(t)$  be the number of connected components of gas at time  $t$ , we set  $B_i(t)$  the  $i$ -th connected component (i.e. bubble number  $i$ ). Let  $\xi$  be a function defined on  $\Lambda \times (0, T)$  negative in  $\Omega(t)$  and equal to  $i$  in bubble  $B_i(t)$ . At each time step we compute  $B_i^n$ ,  $\xi^n$  and  $k^n$ , the approximations of  $B_i(t^n)$ ,  $\xi(t^n)$  and  $k(t^n)$ , as follows.

The function  $\xi^n$  is initialized with color 0 on  $\Lambda \setminus \Omega^n$ ,  $\xi^n = -1$  on  $\Omega^n$ , and  $k^n = 0$ . The gas domain is determined by  $\Xi^n = \{x \in \Lambda \setminus \Omega^n\}$  or  $\Xi^n = \{x \in \Lambda : \xi^n(x) = 0\}$ . The goal is to assign to each point  $x$  in the gas an integer value  $\xi^n(x) \neq 0$ , the so-called *bubble color*. The algorithm is illustrated in Fig. 6 and is the following :

$$\begin{aligned} & \text{Repeat } \left\{ \begin{array}{l} 1. \text{ Choose a point } P \text{ in the interior of } \Xi^n \\ 2. \text{ Solve the following problem} \\ \quad \left\{ \begin{array}{l} -\Delta u = \delta_P, \text{ in } \Xi^n, \\ u = 0, \text{ on } \partial\Xi^n, \end{array} \right. \quad (12) \\ \text{where } \delta_P \text{ is Dirac delta function at point } P; \\ 3. \text{ Increase the number of colors at time } t^n, k^n := k^n + 1; \\ 4. \text{ Define the new connected component } B_{k^n}^n = \{x; u(x) > 0\}; \\ 5. \text{ Set the new color } \xi^n(x) = k^n, \forall x \in B_{k^n}^n; \\ 6. \text{ Define the domain } \Xi^n \text{ for the next iteration} \\ \quad \Xi^n = \{x \in \Lambda \setminus \Omega^n : \xi^n(x) = 0\}. \\ \end{array} \right\} \text{ until } \Xi^n = \emptyset. \end{aligned}$$

The bubble coloration algorithm thus requires to solve as many Poisson problems as the number of connected gas components. However, this is much less CPU time consuming than solving a Stokes problem in the liquid. In our numerical experiments, the CPU time required to compute the bubbles pressure was always less than 10% of the total CPU time.

### 3.3 Diffusion Step

Once the connected components of gas are obtained, a constant pressure  $P^n$  is computed in each connected component. Then the following generalized Stokes problem is solved :

$$\rho \frac{\mathbf{v}^n - \mathbf{v}^{n-\frac{1}{2}}}{\tau^n} - 2\mu \operatorname{div} \mathbf{D}(\mathbf{v}^n) + \nabla p^n = \rho \mathbf{g} \quad \text{in } \Omega^n, \quad (13)$$

$$\operatorname{div} \mathbf{v}^n = 0 \quad \text{in } \Omega^n, \quad (14)$$

with the boundary conditions (4) (5) (6) described in Sect. 2.2.

## 4 Space Discretization and Implementation

Advection and diffusion phenomena being now decoupled, two distinct grids can be used. Since the shape of the cavity  $\Lambda$  can be very complex (this is the case in industrial mould filling situations), finite element techniques are well suited for solving (13) (14) on an unstructured mesh. Furthermore, the pressure in the bubbles is also computed on the same unstructured mesh. On the other hand, a structured grid of smaller cubic cells is used to implement (10) (11) in order to have an accurate approximation of volume fraction of liquid  $\varphi$ .

### 4.1 Advection Step

Assume that the grid is made out of cubic cells of size  $h$ , each cell being labeled by indices  $(ijk)$ . Let  $\varphi_{ijk}^{n-1}$  and  $\mathbf{v}_{ijk}^{n-1}$  be the approximate value of  $\varphi$  and  $\mathbf{v}$  at the center of cell number  $(ijk)$  at time  $t^{n-1}$ . According to (10) and (11), the advection step on cell number  $(ijk)$  consists in advecting  $\varphi_{ijk}^{n-1}$  and  $\mathbf{v}_{ijk}^{n-1}$  by  $\tau^n \mathbf{v}_{ijk}^{n-1}$  and then projecting the values on the structured grid. An example of cell advection and projection is presented in Fig. 7 in two space dimensions.

This method can be interpreted as a forward characteristics method, therefore is unconditionally stable with respect to the Courant-Friedrichs-Lewy (CFL) condition, and  $O(\tau + h^2/\tau)$  convergent according to the theoretical results available for the Characteristics-Galerkin method [21–23]. Since the volume fraction of liquid  $\varphi$  is a step function, this method, as any other method, will smooth the discontinuity. Indeed, numerical diffusion is introduced when the values of the advected cells are projected on the grid. Moreover, if the time step is too large, two cells may arrive at the same place, producing numerical (artificial) compression (in fact (8) develops a shock).

In order to enhance the quality of the volume fraction of liquid, two postprocessing procedures have been implemented. We refer to [12–14] for a detailed description in two and three space dimensions. The first procedure reduces numerical diffusion and is a simplified implementation of the SLIC (Simple Linear Interface Calculation) algorithm [2,19]. The second procedure aims to remove artificial compression, which may result when the time step is too large.

Once values  $\varphi_{ijk}^n$  and  $\mathbf{v}_{ijk}^n$  have been computed on the cells, values of the fraction of liquid  $\varphi_P^n$  and of the velocity field  $\mathbf{v}_P^{n-\frac{1}{2}}$  are computed at the nodes  $P$  of the finite element mesh. When these values are available at the vertices of the finite element mesh, the liquid region is defined as follows. An element of the mesh is said to be liquid if (at least) one of its vertices  $P$  has a value  $\varphi_P^n > 0.5$ . The computational domain  $\Omega^n$  used for solving (13) (14) is then defined to be the union of all liquid elements.

## 4.2 Bubbles

Once the computational liquid domain  $\Omega^n$  is defined, the gas domain is given by  $\Lambda \setminus \Omega^n$ . The connected components of gas are recognized using the algorithm explained in Sect. 3.2 on the finite element mesh. The pressure  $P^n$  is piecewise constant on each connected component and is computed on the gas domain using the method of Sect. 2.3.

## 4.3 Diffusion Step

Let us now turn to the finite element techniques used for solving (13) (14), the boundary conditions (4) (8) (9) being those described in Sect. 2.2. The velocity and pressure are continuous, piecewise linear and a stabilized weak formulation is used [5,6,27], namely for all test functions  $\mathbf{w}$  and  $q$  :

$$\begin{aligned} & \int_{\Omega^n} \frac{\mathbf{v}^n - \mathbf{v}^{n-1/2}}{\tau^n} \mathbf{w} dx + 2\mu \int_{\Omega^n} \mathbf{D}(\mathbf{v}^n) : \mathbf{D}(\mathbf{w}) dx - \int_{\Omega^n} p^n \operatorname{div} \mathbf{w} dx \\ & - \rho \mathbf{g} \int_{\Omega^n} \mathbf{w} dx + \int_{\Gamma^n} (P^n - P_{\text{atmo}}) \mathbf{n} \mathbf{w} dS - \int_{\Omega^n} \operatorname{div} \mathbf{u}^n q dx \\ & - \sum_{K \subset \Omega^n} \alpha_K \int_K \left( \frac{\mathbf{v}^n - \mathbf{v}^{n-1/2}}{\tau^n} + \nabla p^n - \rho \mathbf{g} \right) \cdot \nabla q dx = 0 . \end{aligned}$$

Here  $\mathbf{w}$  and  $q$  are the velocity and pressure test functions, compatible with the boundary conditions on the boundary of the cavity  $\Lambda$ . The stability coefficient  $\alpha_K$  is defined on each tetrahedron  $K$  as a function of the local Reynolds number as follows :

$$\alpha_K = \begin{cases} \frac{1}{12} \frac{h_K^2}{\mu} & \text{if } \frac{\rho |\mathbf{v}^{n-1/2}|_\infty h_K}{2\mu} \leq 3 , \\ \frac{1}{4Re_K} \frac{h_K^2}{\mu} & \text{if } \frac{\rho |\mathbf{v}^{n-1/2}|_\infty h_K}{2\mu} > 3 . \end{cases}$$

Although the above variational formulation corresponds to solving a generalized Stokes problem, numerical experiments reported in [14] have shown that the occurrence of Reynolds number in the definition of the stabilization parameter was necessary. A theoretical justification in a simplified framework (for instance Navier-Stokes equations solved with the Characteristics-Galerkin Least Squares method in a given domain) would be useful but is still missing.

The degrees of freedom are the three velocity components and pressure at each vertex of the finite element mesh. At the moment, all the degrees of freedom are stored in a big matrix. The linear system is solved using a BICGSTAB algorithm and a classical incomplete LU preconditioner. Therefore, the method is memory consuming and decoupling/splitting algorithms such as SIMPLE (see for instance [31] for a recent improvement), Shur

complement (pressure-matrix method), projection methods (pressure Poisson solvers) or inexact LU decompositions should be investigated. However, the two following constraints should be kept in mind before selecting one of these algorithms : i) the decoupling scheme must remain implicit in order to avoid CFL or Fourier-like stability conditions between the time step and the space step, ii) since natural conditions apply on the free surface, the Stokes problem has to be written in conservative form -  $2\mu\text{div } \mathbf{D}(\mathbf{v})$  instead of  $\mu\Delta\mathbf{v}$  - so that the velocity components remain coupled when using splitting algorithms. Some of these decoupling algorithms have been studied in [20].

Once the new velocity field  $\mathbf{v}^n$  is computed at the vertices of the finite element mesh, values are interpolated at the center of the cells ( $ijk$ ). The CPU time spent to interpolate the velocity and volume fraction of liquid between the two grids is negligible compared to the CPU time required to solve Stokes problem. From the implementation point of view, the use of two grids requires an extra data structure. For each cell, the tetraedron number containing the cell is required. Moreover, for each node, the number of the nearest cell has to be stored. The corresponding data structure is set once for all at the beginning of the computation. The size of the cubic cells should be as small as possible, in order to avoid numerical diffusion when advecting the volume fraction of liquid, whereas the size of the finite element mesh can be larger. Numerical experiments reported in [12–14] have shown that choosing the size of the cubic cells three to five times smaller than the size of the finite element mesh is a good compromise between precision and memory requirements.

## 5 Numerical Results

Two and three dimensional results have been proposed in [12] and [13], the influence of gas not being considered. In the sequel, an experiment demonstrating the influence of gas is proposed, namely the S-shape channel. All the computations were performed on a PC with Intel Pentium III 1 Ghz CPU and 512 Mb Memory. The results were post-processed with the CalcoSoft™ software.

An S-shape channel lying between two horizontal plates is filled. The experiment is reported in [25]. A valve is located at the top of the channel, as in Fig. 2, allowing gas to escape. The dimensions of the channel are  $0.17 \times 0.24$  m. Water is injected with velocity 8.7 m/s. In three dimensions, the thickness of the geometry is 0.008 m. The 2D finite element mesh has 3483 vertices and 6418 triangles, while the cells grid contains 49896 cells. The 3D finite element mesh is built using five layers of the 2D mesh (see Fig. 8) and contains 20898 nodes and 96270 elements, while the 3D grid contains 1'544'000 cells. The simulation required 760 time steps of size  $\tau = 0.00007$  s to reach the final time 0.00532 s.

The CPU time for the simulations in two space dimensions is approximately 14 minutes without the bubbles computing and 15 minutes with the bubbles computing. In three space dimensions, these CPU times become 319 minutes without taking into account the gas effect and 344 minutes with the bubbles computing. Most of the CPU time is spent to solve Stokes problem, bubbles computations requiring less than 10% of the total CPU time.

In Fig. 9 the experiment is compared to 2D and 3D computations when the influence of the surrounding gas is not taken into account. Indeed, during the computation, the pressure in the gas remains equal to  $P_{\text{atmo}}$ . Therefore, the bubbles of gas disappear faster in the computation than in the experiment (see for instance the second row of Fig. 9).

The influence of gas is taken into account in Fig. 10. Clearly, the bubbles of gas remain longer in the computations, thus showing that the influence of gas cannot be neglected.

## 6 Conclusion

A two- and three-dimensional free surface flow solver has been presented. The volume fraction of liquid is used to describe the interface. The equations of incompressible flows are solved only in the fluid and the influence of gas is taken into account. A splitting algorithm allows diffusion and convection phenomena to be decoupled. Diffusion is solved with finite elements using an unstructured mesh of tetrahedrons, whereas convection is solved on a grid made out of small cubic cells. Numerical results show the efficiency of this approach, particularly in mould filling situations. Moreover, numerical results show that the pressure in the bubbles of gas has to be taken into account.

We are now investigating the introduction of the surface tension effects in the model. Since the volume fraction of liquid is a step function, the VOF method is not very well suited (compared to level set techniques for instance) to compute the curvature of the free surface. Nevertheless, a number of techniques are available and are constantly being improved [24]. Preliminary results have been obtained but are not included in this paper for the following two reasons: i) due to poor convergence rate, the mesh size has to be very small which prevents accurate computations in 3D, ii) our main interest is to reproduce injection casting processes and the surface tension effects can be neglected for these processes, as the Reynolds number is usually much larger than the Capillary number.

## References

1. Y. C. Chang, T. Y. Hou, B. Merriman, S. Osher : A level set formulation of Eulerian interface capturing methods for incompressible fluid flows. *J. Comput. Phys.* **124** (2) (1996) 449–464
2. A. J. Chorin : Flame Advection and Propagation Algorithms. *J. Comput. Phys.* **35** (1980) 1–11

3. R. Codina, U. Schäfer, E. Oñate : Mould Filling Simulation using Finite Elements. *Int. J. Numer. Meth. Heat Fluid Flow.* **4** (1994) 291–310
4. G. Dhatt, D. M. Gao, A. Ben Cheikh : A Finite Element Simulation of Metal Flow in Moulds. *Int. J. Numer. Meth. Eng.* **30** (1990) 821–831
5. L. P. Franca, S. L. Frey : Stabilized Finite Element Methods : II. The Incompressible Navier-Stokes Equations. *Comp. Meth. Appl. Mech. Eng.* **99** (1992) 209–233
6. L. P. Franca and T. J. R. Hughes : Convergence Analyses of Galerkin Least Squares Methods for Symmetric Advective-Diffusive Forms of the Stokes and Incompressible Navier-Stokes Equations. *Comp. Meth. Appl. Mech. Eng.* **105** (1993) 285–298
7. P. Hansbo : The Characteristic Streamline Diffusion Method for the Time-Dependent Incompressible Navier-Stokes Equations. *Comp. Meth. Appl. Mech. Eng.* **99** (1992) 171–186
8. P. Hansbo : Lagrangian Incompressible Flow Computations in Three Dimensions by Use of Space-Time Finite Elements. *Int. J. Numer. Meth. Fluids.* **20** (1995) 989–1001
9. C. W. Hirt, B. D. Nichols : Volume of Fluid (VOF) Method for the Dynamics of Free Boundaries. *J. Comput. Phys.* **39** (1981) 201–225
10. R. J. LeVeque, K-M. Shyue : Two Dimensional Front Tracking Based on High Resolution Wave Propagation Methods. *J. Comput. Phys.* **123** (1996) 354–368
11. N. Lock, M. Jaeger, M. Medale, R. Ocelli : Local mesh adaptation technique for front tracking problems. *Int. J. Numer. Meth. Fluids.* **28** (1998) 719–736
12. V. Maronnier, M. Picasso, J. Rappaz : Numerical simulation of free surface flows. *J. Comput. Phys.* **155** (2) (1999) 439–455
13. V. Maronnier, M. Picasso, J. Rappaz : Numerical Simulation of Three Dimensional Free Surface Flows. accepted in *Int. J. Numer. Meth. Fluids.*
14. V. Maronnier : Simulation numérique d'écoulements de fluides incompressibles avec surface libre. PHD Thesis **2248**, Département de Mathématiques, Ecole Polytechnique Fédérale de Lausanne. (2000)
15. J. C. Martin, W. J. Moyce : An Experimental Study of the Collapse of Liquid Columns on a Rigid Horizontal Plate. *Philos. Trans. Roy. Soc. London Ser. A* **244** (1952) 312–324
16. F. Mashayek, N. Ashgriz : A Hybrid Finite-Element-Volume-Of-Fluid Method for Simulating Free Surface Flows and Interfaces. *Int. J. Numer. Meth. Fluids.* **20** (1995) 1367–1380
17. M. Medale, M. Jaeger : Numerical simulations of incompressible flows with moving interfaces. *Int. J. Numer. Meth. Fluids* **24** (1997) 615-638
18. F. Muttin, T. Coupez, M. Bellet, J. L. Chenot : Lagrangian Finite-Element Analysis of Time-Dependent Viscous Free-Surface Flow using an Automatic Remeshing Technique: Application to Metal Casting Flow. *Int. J. Numer. Meth. Eng.* **36** (1993) 2001–2015
19. W. F. Noh, P. Woodward : SLIC (Simple Line Interface Calculation). Springer-Verlag, *Lectures Notes in Physics.* **59** (1976) 330–340
20. M. Picasso and J. Rappaz : Stability of time-splitting schemes for the Stokes problem with stabilized finite elements. *Numerical Methods for Partial Differential Equations*, **17-6** (2001) 632-656
21. O. Pironneau : *Finite Element Methods for Fluids*, Wiley, Chichester (1989)

22. O. Pironneau, J. Liou, T. Tezduyar : Characteristic-Galerkin and Galerkin/Least-Squares Space-Time Formulations for the Advection-Diffusion Equation with Time-Dependent Domains. *Comp. Meth. Appl. Mech. Eng.* **100** (1992) 117–141
23. A. Quarteroni, A. Valli : Numerical Approximation of Partial Differential Equations. Springer Series in Computational Mathematics. **23** (1991)
24. Renardy, Yuriko and Renardy, Michael : PROST: a parabolic reconstruction of surface tension for the volume-of-fluid method. *J. Comput. Phys.* **183** (2) (2002) 400–421
25. M. Schmid, F. Klein : Einflußder Wandreibung auf das Füllverhalten Dünnere Platten. Preprint, Steinbeis Transferzentrum, Fachhochschule Aachen. (1996)
26. M. Sussman, A.S. Almgren, J.B. Bell, P. Colella, L.H. Howell, M. L. Welcome : An adaptive level set approach for incompressible two-phase flows . *J. Comput. Phys.* **148** (1) (1999) 81–124
27. T. E. Tezduyar, S. Mittal, S. E. Ray, R. Shih : Incompressible Flow Computations with Stabilized Bilinear and Linear Equal-Order-Interpolation Velocity-Pressure Elements. *Comp. Meth. Appl. Mech. Eng.* **95** (1992) 221–242
28. E. Thompson : Use of Pseudo-Concentrations to Follow Creeping Viscous Flows during Transient Analysis. *Int. J. Numer. Meth. Fluids.* **6** (1986) 749–761
29. S. O. Unverdi, G. Tryggvason : Computations of multi-fluid flows *Physica D.* **60** (1992) 70-83
30. H. Wang, H.K. Dahle, R.E. Ewing, M.S. Espedal, R.C. Sharpley, S. Man : An ELLAM scheme for advection-diffusion equations in two dimensions. *SIAM J. Sci. Comput.* **20** (6) (1999) 2160–2194 (electronic)
31. C. Vuik, A. Saghir, G.P. Boerstoel : The Krylov accelerated SIMPLE(R) method for flow problems in industrial furnaces. *Int. J. Num. Meth. Fluids.* **33** (2000) 1027–1040
32. T. Yabe, T. Ishikawa, P.Y. Wang, I. Aoki, Y. Kadota, F. Ikeda : A universal solver for hyperbolic equations by cubic-polynomial interpolation. II. Two- and three-dimensional solvers. *Comput. Phys. Comm.* **66** (2-3) (1991) 233–242

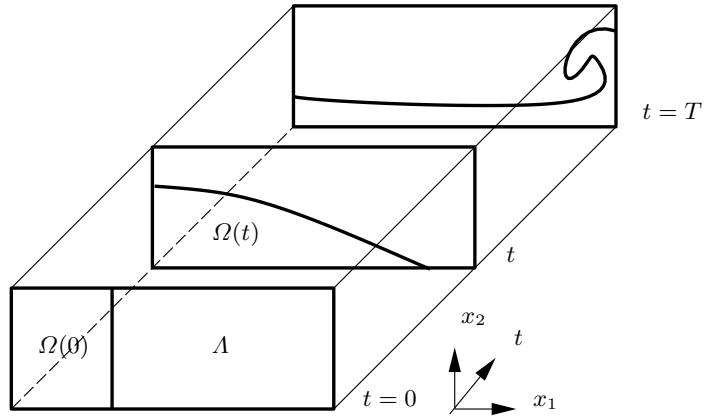


**Fig. 1.** Calculation domain for the broken dam problem in a confined domain. At initial time, the fluid is at rest on the left part of the cavity. It is then free to move and hits the boundary.

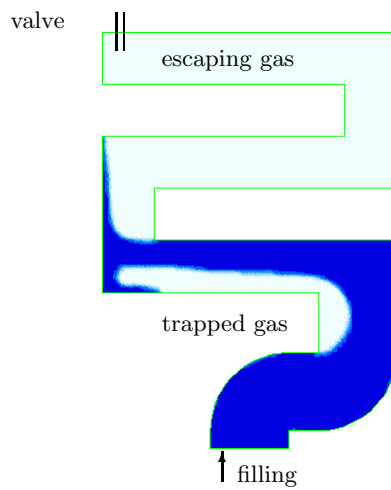


**Fig. 2.** Filling of an S-shaped cavity. The gas in the upper part of the cavity is free to escape from the valve. The gas trapped by the liquid may exert a force on the liquid.

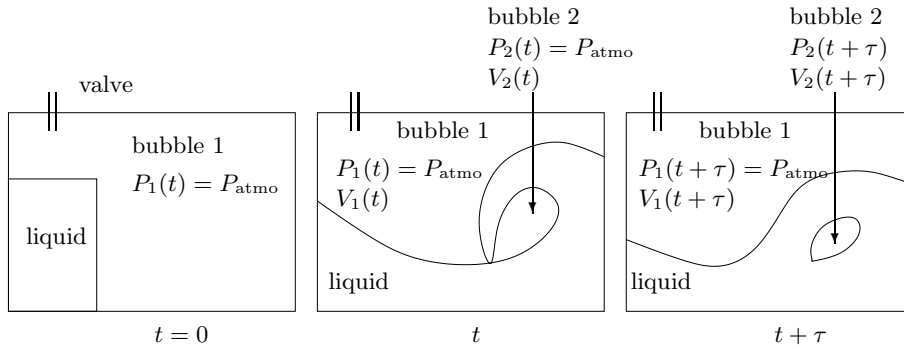


**Fig. 3.** At time  $t$ , air is trapped by the liquid and the pressure equals to atmospheric pressure. ( $P_1(t) = P_{\text{atmo}}$ ,  $P_2(t) = P_{\text{atmo}}$ ). At time  $t + \tau$ , the pressure in bubble 2 is computed from the relation  $P_2(t + \tau)V_2(t + \tau) = P_2(t)V_2(t)$ .

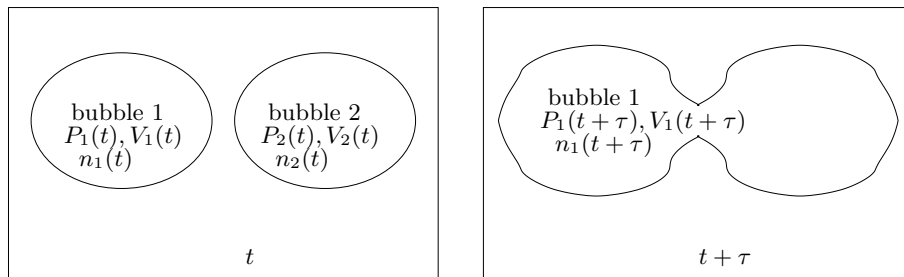


**Fig. 4.** Merging of two bubbles between time  $t$  and time  $t + \tau$ . The pressure in bubble 1 at time  $t + \tau$  is computed from the relation  $P_1(t + \tau)V_1(t + \tau) = P_1(t)V_1(t) + P_2(t)V_2(t)$ .

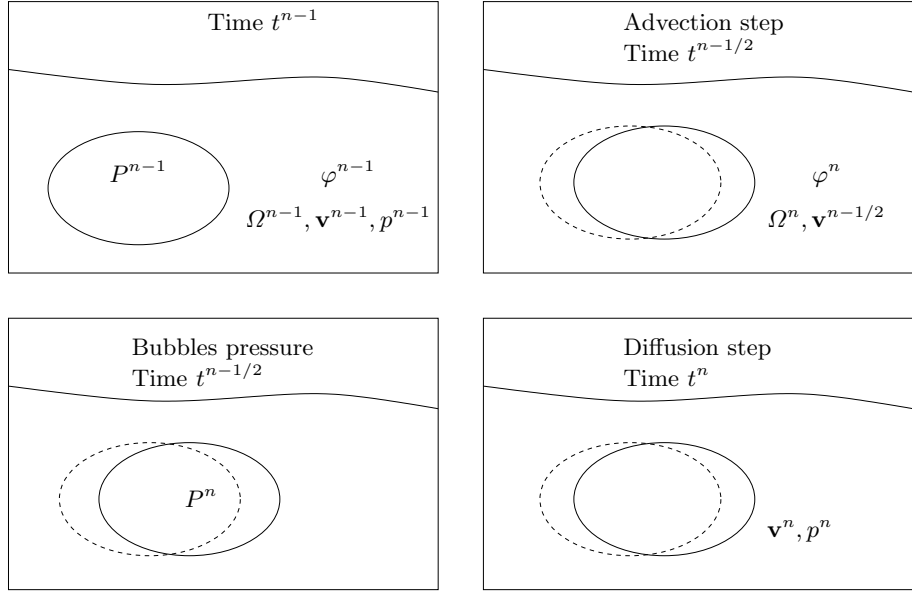


**Fig. 5.** The splitting algorithm. Two advection problems are solved to determine the new volume fraction of liquid  $\varphi^n$ , the new domain  $\Omega^n$  and the predicted velocity  $\mathbf{v}^{n-1/2}$ . Then a constant pressure  $P^n$  is computed in each connected component of gas. Finally, a Stokes problem is solved to obtain the velocity  $\mathbf{v}^n$  and the pressure  $p^n$  in the fluid.

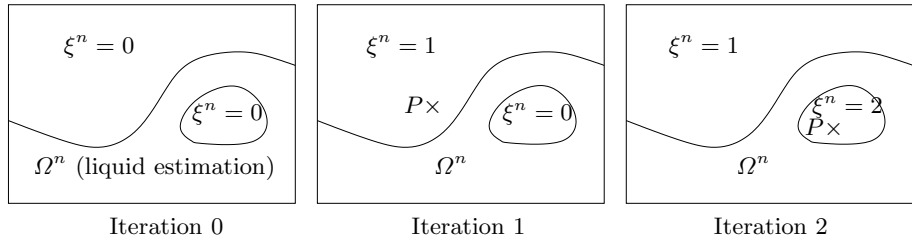


**Fig. 6.** Coloration algorithm of the bubbles. Initially the function  $\xi^n$  equals zero everywhere in the gas. At each iteration of the algorithm a point  $P$  is chosen in the domain where  $\xi^n = 0$ . Then problem (12) is solved and a connected component is found. The algorithm stops when all points in the gas have a color  $\xi^n \neq 0$ .

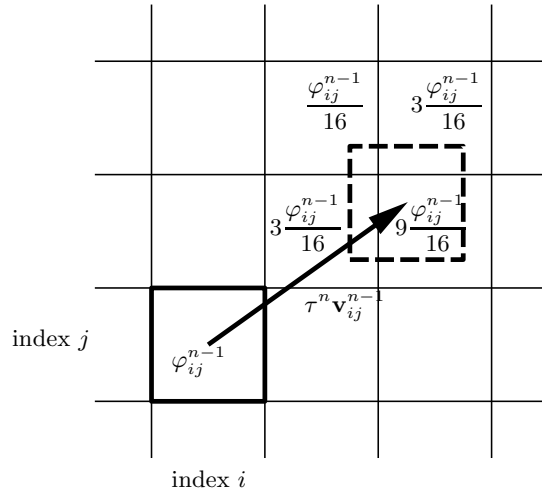


**Fig. 7.** An example of two dimensional advection of  $\varphi_{ij}^{n-1}$  by  $\tau^n \mathbf{v}_{ij}^{n-1}$ , and projection on the grid. The advected cell is represented by the dashed lines. The four cells containing the advected cell receive a fraction of  $\varphi_{ij}^{n-1}$ , according to the position of the advected cell.

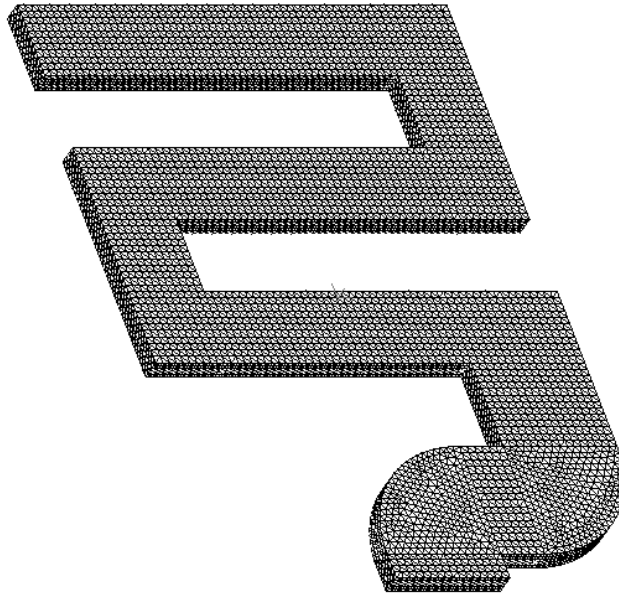


**Fig. 8.** The 3D mesh used for the computations of the S-shape channel.

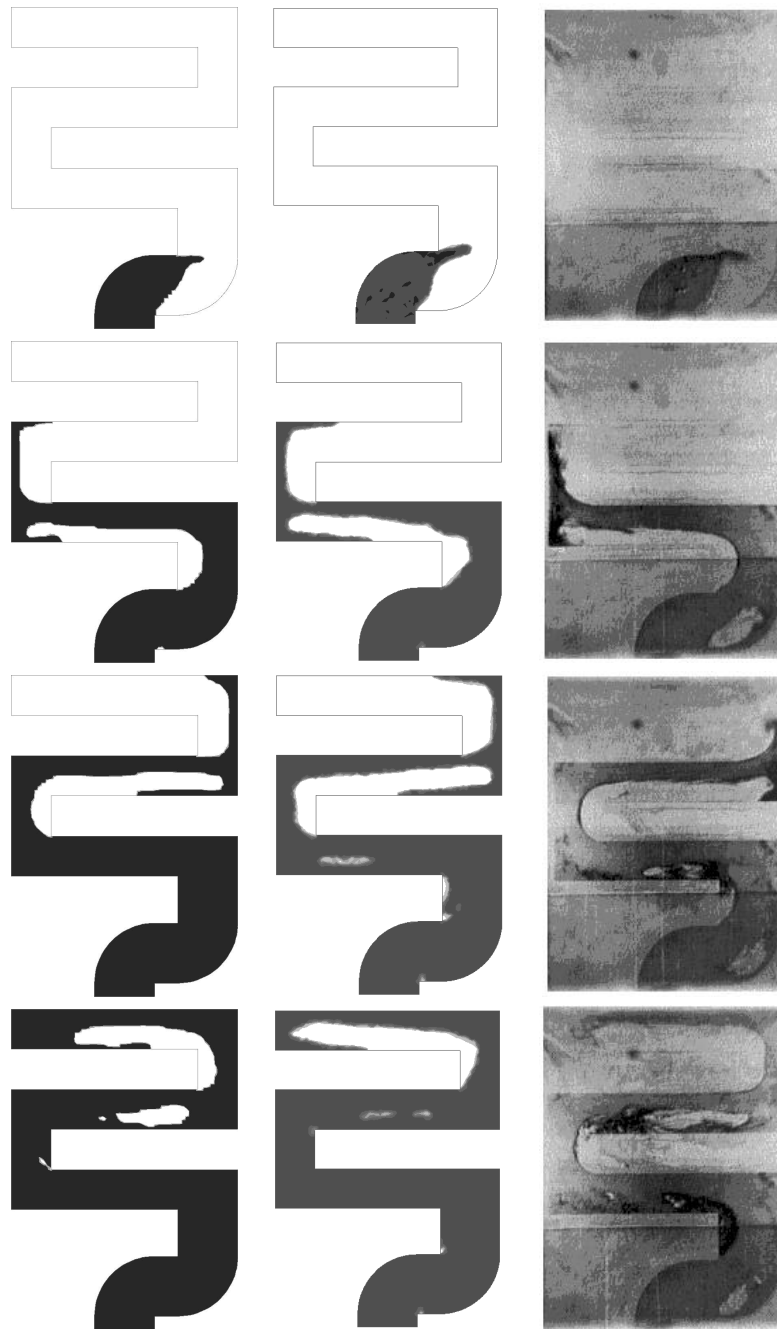


**Fig. 9.** S-shaped channel without influence of gas : left : 2D results, middle : 3D results in a cut, right : experimental results [25]. First row : time equals 7.15 ms, second row : 25.3 ms, third row : 39.3 ms and fourth row : 53.6 ms.

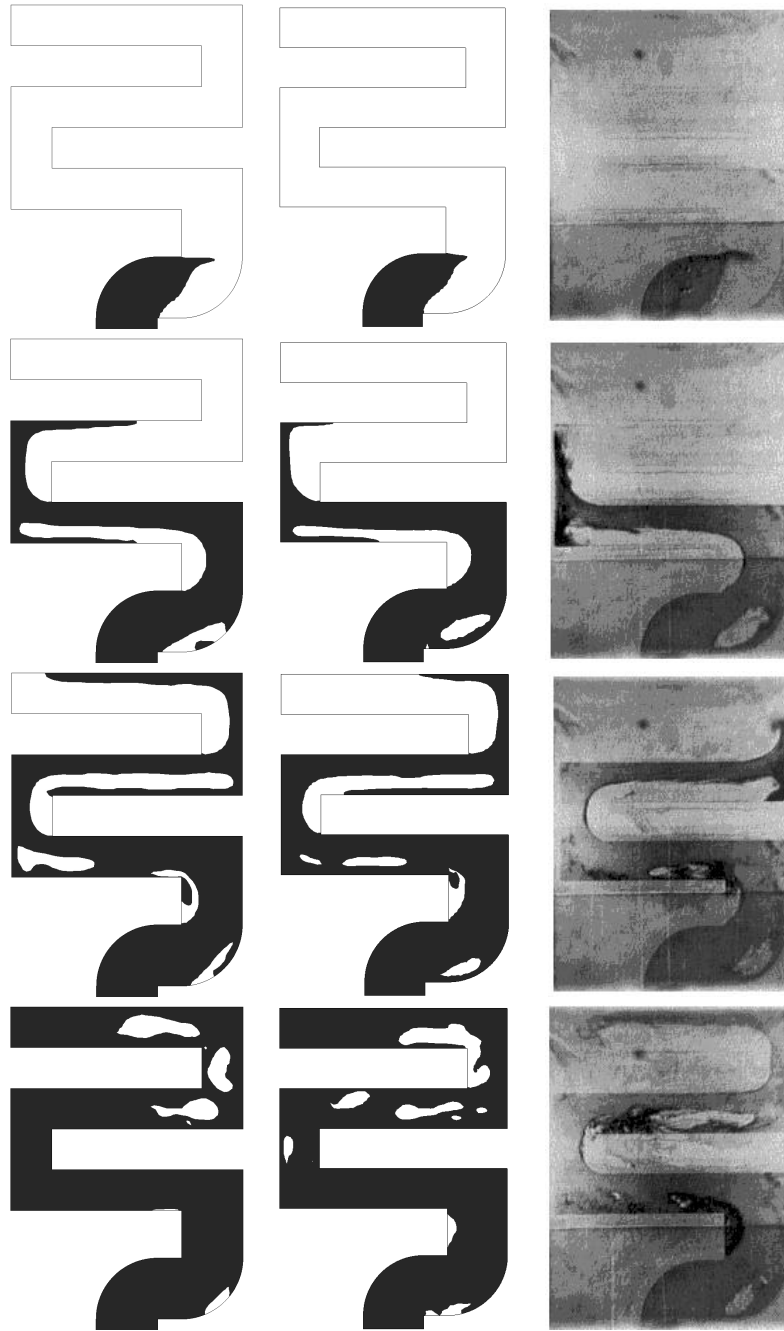


**Fig. 10.** S-shaped channel with influence of gas : left : 2D results, middle : 3D results in a cut, right : experimental results [25]. First row : time equals 7.15 ms, second row : 25.3 ms, third row : 39.3 ms and fourth row : 53.6 ms.